Patupilone-loaded poly(L-glutamic acid)-*graft*-methoxy-poly(ethylene glycol) micelle for oncotherapy

Jing Yan, Dawei Zhang, Haiyang Yu, Lili Ma, Mingxiao Deng, Zhaohui Tang & Xuefei Zhang

Taylor & Francis
Taylor & Francis Group

Patupilone-loaded poly(L-glutamic acid)-*graft*-methoxy-poly(ethylene glycol) micelle for oncotherapy
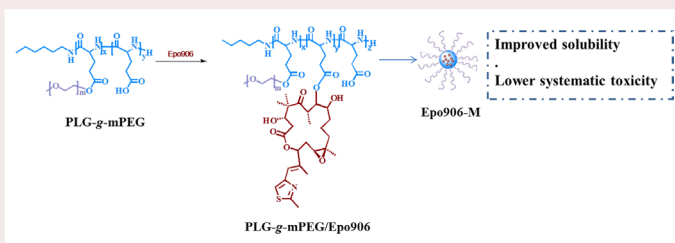
Jing Yan[a,c] (iD), Dawei Zhang[c], Haiyang Yu[c], Lili Ma[c], Mingxiao Deng[d], Zhaohui Tang[c] and Xuefei Zhang[a,b]

[a]Department of Chemistry, Xiangtan University, Xiangtan, PR China; [b]Key Laboratory of Environmentally Friendly Chemistry and Applications of Ministry of Education, Key Laboratory of Polymeric Materials and Application Technology of Hunan Province, Xiangtan University, Xiangtan, PR China; [c]Key Laboratory of Polymer Ecomaterials, Changchun Institute of Applied Chemistry, Chinese Academy of Sciences, Changchun, PR China; [d]College of Chemistry, Northeast Normal University, Changchun, PR China

ABSTRACT

Patupilone, an original natural anti-cancer agent, also known as epothilone B or Epo906, has shown promise for the treatment of a variety of cancers, however, the systematic side effects of patupilone significantly impaired its clinical translation. Herein, patupilone-loaded PLG-*g*-mPEG micelles were prepared. Patupilone was grafted to a poly(L-glutamic acid)-*graft*-methoxy-poly(ethylene glycol) (PLG-*g*-mPEG) by Steglich esterification reaction to give PLG-*g*-mPEG/Epo906 that could self-assemble to form patupilone-loaded micelles (Epo906-M). The Epo906-M was able to inhibit the proliferation of A549, MCF-7 cancer cells and BEAs-2B cells *in vitro*. For *in vivo* treatment of orthotopic xenograft tumor models (MCF-7), the Epo906-M exhibited higher tumor inhibition efficiency with lower side effects as compared with free Epo906. Seventeen percent of the body weight loss appeared in the group treated with free Epo906 of 0.25 mg kg^{-1}, while the group treated with Epo906-M of 10 mg kg^{-1} showed less than ten percent of body weight loss and displayed stronger tumor inhibiting effect. Therefore, the polypeptide-patupilone conjugate has improved potential for oncotherapy.

Patupilone-loaded poly(L-glutamic acid)-graft-methoxy-poly(ethylene glycol) micelle (Epo906-M) was prepared. The Epo906-M shows improved solubility and lower systemic toxicity than free patupilone.

PLG-*g*-mPEG → Epo906 → PLG-*g*-mPEG/Epo906 → Epo906-M | Improved solubility | Lower systematic toxicity

---

CONTACT Zhaohui Tang ✉ ztang@ciac.ac.cn; Xuefei Zhang ✉ zxf7515@163.com

1. Introduction

Microtubules are a validated and well established target in cancer therapy because of their essential role during mitosis [1,2]. Microtubulin inhibitors lead to cell apoptosis by disturbing the balance of microtubule. This is the case in particular for rapidly proliferating cancer cells where minor changes of the microtubular equilibrium produce major impact [3,4]. Epothilones, one class of the microtubulin inhibitors, are a novel class of natural cytotoxic compounds, originally isolated from the myxobacterium Sorangium cellulosum in the early 1990s [3,5,6]. Epothilones kill tumor cells through a mechanism of action similar to that of paclitaxel, namely through induction of tubulin polymerization to microtubules and microtubule stabilization [7].

Patupilone, also called epothilone B or EPO906, is one of the natural epothilones, which is currently in phase III clinical trials for the treatment of advanced ovarian cancer [8,9]. In comparison to paclitaxel, patupilone has less complex molecular structure and a broader antineoplastic spectrum. In some anti-cancer experiments, patupilone revealed a 2000 ± 5000-fold higher potency than paclitaxel [10], a striking enough observation to awaken and stimulate the interest of many in the academic community and the pharmaceutical industry. Additionally, patupilone (as well as a number of its analogs) has been demonstrated to possess potent *in vivo* antitumor activity in a number of multidrug-resistant human tumor models in mice [10–13].

Though there are so many advantages for the patupilone, it has some shortages [14]. Firstly, patupilone has poor solubility in aqueous solutions [15], so that adjuvants must be used to improve its water solubility. Whereas, currently used solubilizer like Cremophor EL [16] has been implicated in clinically severe adverse effects and unfavourable alterations of the pharmacokinetics of drugs [17] as shown for paclitaxel [18]. Secondly, patupilone does harm to normal cells at some extent [19]. Patupilone shows severe gastrointestinal side effects in treatment of patients with castration-resistant prostate cancer in clinical trials [20]. General toxicities (anorexia, asthenia, dehydration, pain in extremity), gastrointestinal side effects (diarrhea, nausea, vomiting, abdominal pain, flatulence) and neurological toxicity (neuropathy) were also shown in a phase I dose escalation trial for patients with pretreated advanced/metastatic colon cancer [21]. Similar toxicities have been seen in the treatments of refractory or resistant patients with recurrent epithelial ovarian, primary fallopian tube [8], and patients with brain metastases from breast cancer [22] using patupilone. A dose-limiting toxicity (pneumonia for a relatively lower dose, renal failure and pulmonary hemorrhage for a relatively higher dose) was observed [23]. Last but not least, it is unstable in blood circulation [13].

Nanotechnology confer nanomedicines with many advantages [24], such as lower side effects of chemotherapeutic agents [25], longer cycling time in blood circulation [26], improving stability [27], solubility [28] and biocompatibility [29–31]. Meanwhile, nanoparticles of size between 20 and 200 nm would accumulate in the solid tumor because of the enhanced permeability and retention (EPR) effect [32–34].

Up to now, few attempts have been made to prepare polymer-patupilone conjugate nanomedicine. For example, Zhang and co-workers [35] attempted to prepare a series of PEG-Epo906 conjugates by mPEG with different molecular weights. The water solubility of the PEG-Epo906 was significantly improved as compared with patupilone, however, a large amount of PEG is necessary in order to administer an effective amount of the drug because only one molecule of the patupilone can be bound to one molecule of mPEG for structural reason. In the present study, poly(glutamic acid)-*graft*-methoxy-poly(ethylene glycol) (PLG-*g*-mPEG) was used to conjugate patupilone (PLG-*g*-mPEG/Epo906).

Because of the existence of a large number of carboxylic acid groups on the main chain of the PLG-*g*-mPEG, high drug loading content was expected for the PLG-*g*-mPEG/Epo906. The systematic toxicity effect, *in vitro* and *in vivo* anti-tumor efficacy of the PLG-*g*-mPEG/Epo906 were evaluated in details.

2. Materials and methods

2.1. Materials

Patupilone (Epothilone B, Epo906) was purchased from Zhejiang Haisun Pharmaceutical Co., Ltd. and used as received. 4-dimethylaminopyridine (DMAP, Alfa Aesar) was used without further purification. 3-(45-dimethyl-thiazol-2-yl)-25-diphenyl tetrazolium bromide (MTT) and 4',6-diamidino-2-phenylindole dihydrochloride (DAPI) were both purchased from Sigma-Aldrich and used as received. Fluorescein isothiocyanate (FITC) was purchased from Aladdin Reagent Co., Ltd. N,N-dimethylformamide (DMF) was stored with calcium hydride (CaH_2) and purified by vacuum distillation over CaH_2. IR830-B-NH_2 was prepared as previous work [36]. All other reagents and solvents were purchased from Sinopharm Chemical Reagent Co., Ltd. and used as received. Purified deionized water was prepared by the Milli-Q plus system (Millipore Co., Billerica, MA, USA).

2.2. Characterization

^{1}HNMR spectra were recorded on a Bruker AV 400NMR spectrometer in trifluoro-acetic acid-*d* (CF_3COOD). UV–vis was measured on a UV-2401 PC spectrophotometer (Shimadzu). Dynamic laser scattering (DLS) measurement was performed on a Wyatt QELS instrument with a vertically polarized He–Ne laser (DAWN EOS, Wyatt Technology, USA). The scattering angle was fixed at 90°. Transmission electron microscopy (TEM) measurement was performed on a JEOL JEM-1011 transmission electron microscope with an accelerating voltage of 100 kV. Critical micelle concentration (CMC) was estimated by fluorescence spectroscopy using pyrene as the probe, following our previous method [37]. Confocal laser scanning microscopy (CLSM) observations were carried out using Carl Zeiss LSM 780. Fluorescence-activated cell sorter (FACS) was performed by flow cytometer (Beckman, California, USA). Optoacoustic imaging was presented on a multispectral optoacoustic tomography (MSOT) scanner with 128 ultrasound transducer elements equipped (MSOT inVision 128, iThera Medical GmbH, Munich, Germany). The histological alterations were observed by microscopy (Nikon TI-S/L100).

2.3. Synthesis of PLG-g-mPEG/Epo906

PLG-*g*-mPEG with an average of 160 L-glutamic acid repeating units and a mean of 8.3 mPEG5 K chains was synthesized as our previous work [38–40]. PLG-*g*-mPEG/Epo906 was synthesized through a Steglich esterification reaction between PLG-*g*-mPEG and Epo906 using diisopropyl-carbodiimide (DIC) and 4-dimethylaminopyridine (DMAP) as condensing agent and catalytic agent, respectively. In brief, PLG-*g*-mPEG (3.400 g, 0.055 mmol), Epo906 (0.600 g, 1.182 mmol) and DMAP (0.072 g, 0.591 mmol) were weighted and added into a flask which was flame-dried for three times and purged with nitrogen. Dry DMF (58 mL) and DIC (0.446 g, 3.546 mmol)

was then added. After the reaction was carried out under stirring and with nitrogen protection at room temperature for 24 h, the reaction mixture was precipitated into excess amount of cold ether for 3 times to give PLG-*g*-mPEG/Epo906 crude product. The crude product was then redissolved in DMF and dialyzed against DMF (MWCO = 7000 Da) to remove free Epo906. The purified PLG-*g*-mPEG/Epo906 was obtained as a white cotton-like solid by dialyzing against distilled water (MWCO = 7000 Da) and freeze-drying subsequently.

For evaluating the loading content and loading efficiency of Epo906, lyophilized PLG-g-mPEG/Epo906 was dissolved in N,N′-dimethylformamide (DMF) and measured by UV–vis spectrometer at 280 nm. Drug loading content (DLC) and drug loading efficiency (DLE) were calculated according to the following formulas:

DLC (wt%) = (weight of loaded Epo906/weight of PLG-*g*-mPEG/Epo906) × 100%
DLE (wt%) = (weight of loaded Epo906/weight of feeding Epo906) × 100%

2.4. Preparation of the fluorescent isothiocyanate (FITC) labeled PLG-g-mPEG/Epo906

The FITC labeled PLG-*g*-mPEG/Epo906 was prepared by the reaction of isothiocyanate group of FITC with free amino group in the end of poly(glutamic acid) chain of PLG-*g*-mPEG/EPO906. In brief, PLG-*g*-mPEG/EPO906 lyophilized powder (150.0 mg) and FITC (5.0 mg) were dissolved in DMF (8.0 mL) and stirred overnight in the dark at room temperature. The resultant reactant solution was purified by dialyzing against deionized water under dark for 96 h (MWCO = 3500 Da) to obtain FITC-labeled PLG-*g*-mPEG/Epo906. After lyophilization, a light yellow floccule was obtained and stored in dark before use.

2.5. Preparation of the IR830-labeled PLG-g-mPEG/Epo906

The IR830-labeled PLG-*g*-mPEG/Epo906 was prepared by the reaction of PLG-*g*-mPEG/Epo906 with IR830-B-NH$_2$ at a feeding molar ratio of 1/2 in DMF solvent. After the PLG-*g*-mPEG/Epo906 was activated by carbodiimide hydrochloride (EDC·HCl) and 1-hydroxy benzotriazole (HOBT) (molar ratio of the PLG-*g*-mPEG/Epo906/EDC·HCl/HOBT was 1/4/4) with stirring for 30 min in the dark at room temperature, the IR830-B-NH$_2$ was added with one equivalent of DMAP. After reacting at room temperature for 24 h, dialyzing against deionized water (MWCO = 3500 Da) and lyophilizing, IR830 labeled PLG-*g*-mPEG/Epo906 was obtained.

2.6. Measurement of CMC

The CMC of the PLG-*g*-mPEG/Epo906 solution was assessed by fluorescence spectroscopy using pyrene as the probe, with excitation spectra of 300–360 nm and emission wavelength of 390 nm set. The intensity ratios of the third (339 nm) vibronic peaks to the first (335 nm) ones of pyrene fluorescence were plotted as a function of logarithm of polymer concentration, and CMC was calculated in accord with the turning point concentration [41].

2.7. Stability of PLG-g-mPEG/Epo906

The stability of the PLG-*g*-mPEG/Epo906 micelle was evaluated by DLS. Epo906-M was dissolved in phosphate buffered saline (PBS) solution at different pH (7.4 or 5.5). The samples were kept at 37 °C with a shaking rate of 90 rpm. Then, at different time intervals (0, 1, 3, 6, 12, 24, 36, 48, 72 h), the hydrodynamic radius (R_h) was determined by DLS.

2.8. Cell cultures

The human breast cancer cells (MCF-7), the human lung carcinoma (A549) cells and human bronchial epithelial cells (BEAs-2B) were cultured at 37 °C in a 5% CO_2 atmosphere. Dulbecco's modified Eagle's medium (DMEM, Gibco) for MCF-7, A549 cells and RPMI 1640 medium (Gibco) for BEAs-2B cells supplemented with 10% fetal bovine serum, penicillin (50 U mL^{-1}) and streptomycin (50 U mL^{-1}) were used as culture medium.

2.9. Cellular uptake study

The cellular uptake of FITC labeled PLG-*g*-mPEG/Epo906 was evaluated by confocal laser scanning microscopy (CLSM) and FACS against MCF-7 cells. The quantification of the cellular uptake for both free Epo906 and Epo906-M is evaluated by HPLC.

2.10. Confocal laser scanning microscopy

The cellular uptake of the FITC labeled PLG-*g*-mPEG/Epo906 was determined by confocal laser scanning microscopy toward MCF-7 cells. The cells were seeded in 6-well plates at 1.0×10^5 cells per well in 2.0 mL DMEM and cultured for 24 h, and then incubated for another 1, 3 or 6 h with FITC-labeled PLG-*g*-mPEG/Epo906 at 37 °C. Thereafter, the culture medium was taken out and cells were washed with PBS (0.01 M, pH = 7.4) for three times (5 min per time). Then, the cells were fixed with 4% (w/v) paraformaldehyde for 25 min at 25 °C, after washing for 5 times with PBS, the cell nuclei were stained with 46-diamidino-2-phenylindole (DAPI) according to the standard protocols from the supplier. CLSM images were taken by a laser scanning confocal microscope.

2.11. Flow cytometry

MCF-7 cells were seeded in 6-well plates with a density of 3×10^5 cells per well in 2.0 mL of complete DMEM and cultured for 24 h, then incubated at 37 °C for additional 1 or 3 h with the FITC-labeled PLG-*g*-mPEG/Epo906 in the same concentration as the CLSM used. Soon after the culture media was removed, cells were washed with PBS (0.01 M, pH = 7.4) thrice and the trypsin was added. Subsequently, 0.5 mL PBS (0.01 M, pH = 7.4) was added to each well, and the solutions were centrifuged at 3000 rpm for 5 min. After that, with removal of the supernatants, the cells were resuspended in 0.3 mL PBS (0.01 M, pH = 7.4). Data were analyzed and performed by software FlowJo.

2.12. Quantification of cell uptake study

MCF-7 cells were seeded in 6-well plates with a density of 3×10^5 cells per well in 2.0 mL of complete DMEM and cultured for 24 h. The culture medium was removed and each well was added with 2.0 mL of PBS. MCF-7 cells were then incubated at 37 °C for additional 1, 3 or 6 h with free Epo906 (in PBS, pH = 7.4) or PLG-g-mPEG/Epo906 (in PBS, pH = 7.4) with the same drug concentration of 50 μg mL^{-1} at the basis of free Epo906. The PBS phase was collected and filtrated through 0.22 μm membrane. The amount of free EPO906 or PLG-g-mPEG/Epo906 in the PBS solution was determined by HPLC. The amount of drug that was uptaken by MCF-7 cells was determined by the amount of feeded drug minus the remained drug in the PBS solution.

2.13. Cytotoxicity assay

The relative cytotoxicities of free EPO906 and PLG-g-mPEG/Epo906 were evaluated by measuring the cell viability through the MTT assay and Trypan blue exclusion assay.

2.13.1. MTT assay

The MCF-7 and A549 cells were seeded in 96-well plates (both with 6.0×10^3 cells per well) in 180 μL of complete DMEM containing 10% fetal bovine serum, supplemented with 50 U mL^{-1} penicillin and 50 U mL^{-1} streptomycin, and incubated at 37 °C in 5% CO_2 atmosphere for 24 h. The culture medium was replaced with 180 μL of fresh medium containing free Epo906 and PLG-g-mPEG/Epo906 at different concentrations. Followed by 48 and 72 h incubation, 20 μL of MTT solution (5 mg mL^{-1} in PBS) was added in each well. With incubation for additional 4 h, all the 200 μL solution were withdrawn and replaced with 150 μL DMSO.

The BEAs-2B cells were seeded in 96-well plate with RPMI 1640 medium at a density of 5.0×10^3 per well for 48 or 72 h with the similar procedure to the above MTT assays.

The absorbance of the solution was measured with a Bio-Rad 680 microplate reader at 490 nm. Cell viability (%) was calculated on the basis of the following equation:

cell viability (%) = $(A_{sample}/A_{control}) \times 100\%$, where A_{sample} and $A_{control}$ represented the absorbance of the sample well and the control well, respectively.

2.13.2. Trypan blue exclusion assay

The MCF-7 cells were seeded in 6-well plate in 3.0 mL of complete DMEM containing 10% fetal bovine serum, supplemented with 50 U mL^{-1} penicillin and 50 U mL^{-1} streptomycin, and incubated at 37 °C in 5% CO_2 atmosphere for 24 h. The culture medium was replaced with 2.0 mL of fresh medium containing free Epo906 and PLG-g-mPEG/Epo906 at different concentrations. After 48 h incubation, cells were harvested using trypsin and stained with 0.4% trypan blue dye. Total cell counts and viable cell numbers were determined with a microscope. The cell viability (%) = the amount of the living cells/(the total amount of the living cells and dead cells) × 100%.

2.14. In vivo distribution

MSOT was used to evaluate the *in vivo* distribution. Balb/C nude mice (body weight 16.0 g) bearing MCF-7 orthotopic xenograft tumors (500–700 mm³) were injected with

IR830-labeled PLG-*g*-mPEG/Epo906 (dose: 15 mg kg^{-1} equivalent weight of Epo906) via intravenous injection. After different time intervals (1, 4, 24, 48, 72 h), the mice were anaesthetized with 2% isoflurane and put into the MSOT system. Multispectral process scanning (MSP) was carried out at 680 nm, 835 and 900 nm. The results were reconstructed with a linear model, and linear regression was used for the multispectral processing.

2.15. In vivo *antitumor efficiency*

Balb/C nude mice (6 weeks old, female), with an average body weight around 18 g, were purchased from Beijing Vitalriver Experimental Animal Technology Co., Ltd. and raised in a specific pathogen-free (SPF) animal lab. All the animal experiments were approved by the Animal Care and Use Committee of Jilin University. The anti-tumor efficacy of free drugs and drug-loaded micelles were assessed by MCF-7 orthotopic human breast carcinoma on female Balb/C nude mice. The orthotopic xenograft model was established by *in situ* injection of 2.0×10^6 MCF-7 cells (100 μL in PBS) into the mammary fat pad nearing the hind leg of each mouse. When the tumor volume reached approximately 50–100 mm^3, mice were divided into 4 groups ($n = 6$) randomly, the day was appointed as day 0. Mice were treated with PBS, free Epo906 (0.25 mg kg^{-1}), free Epo906 (0.50 mg kg^{-1}), and Epo906-M (10 mg kg^{-1} equivalent weight of Epo906) intravenously via tail vein on days 0, 2, 4, and 6. Tumor volume and body weight were measured every other day to assess the antitumor activities and systematic toxicities of various groups. The probable tumor volume (mm^3) was calculated based on the following equation:

$$V = a \times b^2/2$$

where a and b represented the longest and shortest diameter of tumors, respectively.

At day 18, mice were euthanized. Tumors and major organs, including heart, liver, spleen, lung and kidney were excised for histopathology analyses.

2.16. *Histopathology analysis*

The hematoxylin and eosin (H&E) staining method was used to evaluate the histopathological damage. Briefly, at day 18, mice were anesthetized and the chests were cut open. From the left atrium, PBS (0.01 M, pH = 7.4) and paraformaldehyde solution (4% in) were perfused. Tumors were fetched and fixed in 4% buffered paraformaldehyde overnight, and then embedded in paraffin. The paraffin-embedded tissue samples of the tumors were sliced at 5 μm thickness, and stained with H&E for histopathological changes evaluation using microscope (Nikon TE2000U).

2.17. *Data analysis*

All the experiments were performed at least three times and expressed as means ± SD. Data were analyzed for statistical significance using one-way ANOVA test. $p < 0.01$ was considered highly significant, and $p < 0.05$ was considered statistically significant.
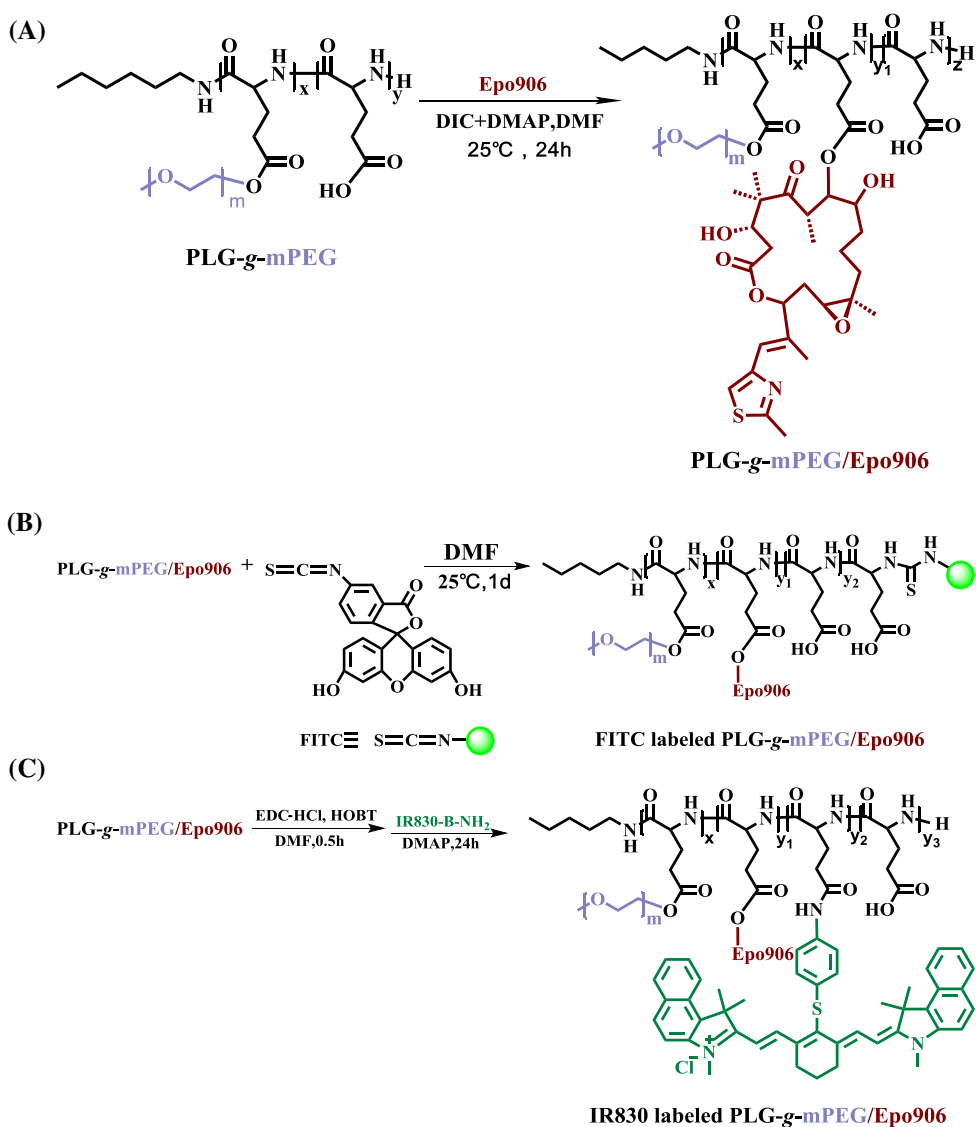
Scheme 1. Preparation of (A) PLG-*g*-mPEG/Epo906, (B) FITC-labeled PLG-*g*-mPEG/Epo906 and (C) IR830-labeled PLG-*g*-mPEG/Epo906.

3. Results and discussion

3.1. Preparation PLG-g-mPEG/Epo906

PLG-*g*-mPEG has been shown to be a biodegradable polymeric carrier that can significantly prolong the blood circulation time of payloads and improve the tumor targetability of nanomedicines *in vivo* [38–40,42–45]. Considering that ester bonds have been successfully used for the conjugation of Epo906 to PEG, poly(L-glutamic acid)-*graft*-methoxy-poly(ethylene glycol) patupilone conjugate PLG-*g*-mPEG/Epo906 was prepared by the Steglich esterification reaction of the PLG-*g*-mPEG with patupilone (Scheme 1(A)). The ^{1}HNMR spectra of the PLG-*g*-mPEG/Epo906 and PLG-*g*-mPEG in CF$_3$COOD
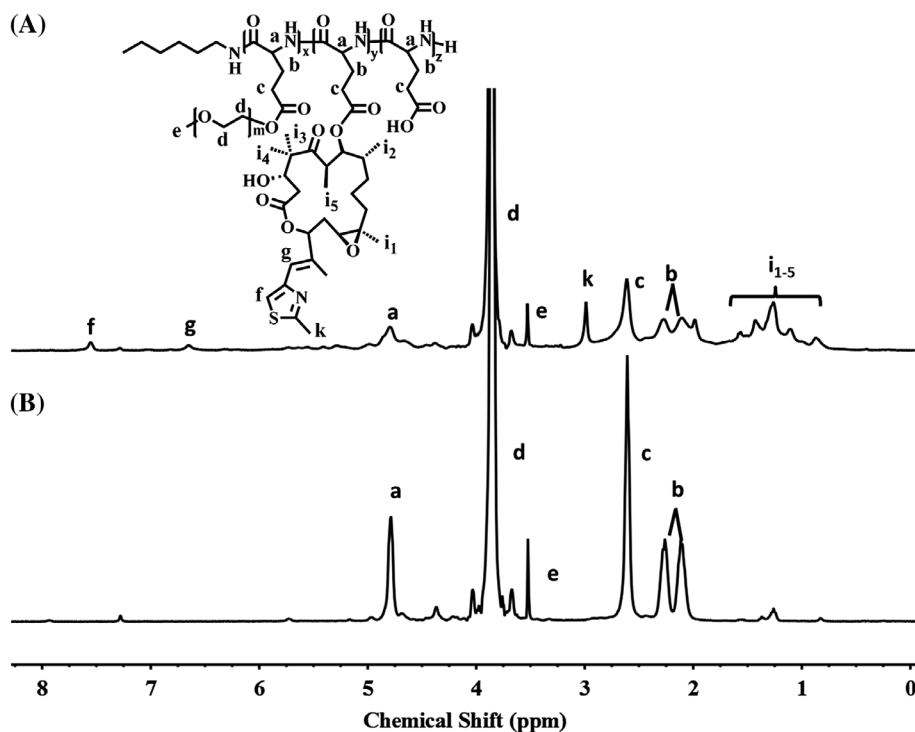
Figure 1. ¹HNMR spectra of (A) PLG-*g*-mPEG/Epo906 and (B) PLG-*g*-mPEG in CF₃COOD.

Table 1. GPC analysis of PLG-*g*-mPEG/Epo906.

Polymers	$Mn \times 10^{-3}$(g mol⁻¹)	PDI
PLG-*g*-mPEG/Epo906	34.2	1.50

were shown in Figure 1. The appearance of the characteristic peaks f (thiazole protons of Epo906, δ 7.55 ppm) and g (double bond protons of Epo906, δ 6.65 ppm) in the ¹HNMR spectrum of PLG-*g*-mPEG/Epo906 (Figure 1(A)) indicated that Epo906 was successfully grafted to the PLG-*g*-mPEG. The obtained conjugates PLG-*g*-mPEG/Epo906 had a Mn of 34.2×10^3 g mol⁻¹ and PDI of 1.50, as determined by GPC, as shown in Table 1. The CMC of the PLG-*g*-mPEG/Epo906 micelles (Epo906-M) was 16.93 ng mL⁻¹ (Figure 2), measured by fluorescence spectroscopy using pyrene as the probe. The DLC of the Epo906-M was 14.6 wt% by the UV–vis, which was much higher than those of PEG5 K-Epo906 (DLC = 7.19 wt%) and PEG20 K-Epo906 (DLC = 1.82 wt%) [35]. The DLE of the Epo906-M was 97.7%, indicating that the high efficiency of the grafting reaction of Epo906 to the poly(glutamic acid) backbone.

HPLC curves of PLG-*g*-mPEG/Epo906 (A), PLG-*g*-mPEG (B) and Epo906 (C) were showed in Figure 3. The peaks of the PLG-*g*-mPEG at 1.47 min and Epo906 at 3.37 min were not appeared in the spectrum of the PLG-*g*-mPEG/Epo906, which further proved that PLG-*g*-mPEG/Epo906 was prepared successfully without residual free Epo906.
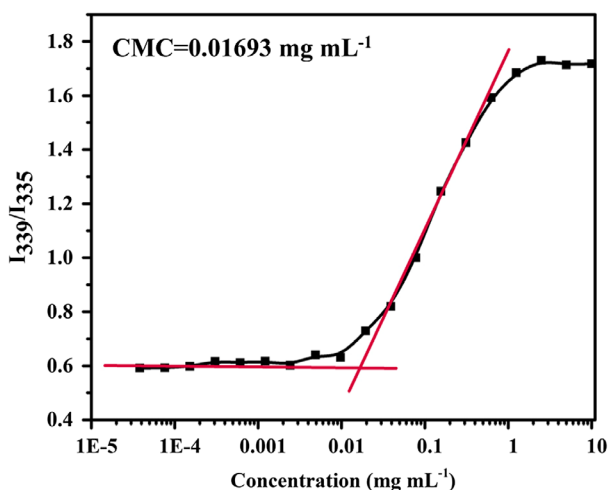
Figure 2. Dependence of excitation fluorescence intensity ratio of pyrene (I_{339}/I_{335}) on the logarithmic concentration of PLG-*g*-mPEG/Epo906.
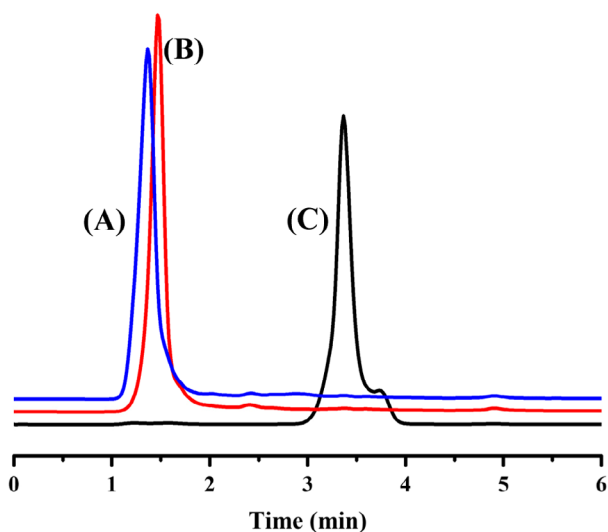

Figure 3. HPLC spectra of PLG-g-mPEG/Epo906 (A), PLG-*g*-mPEG (B), and Epo906 (C).
Note: The mobile phase was acetonitrile and water (v_1/v_2=4:1).

The hydrodynamic radius (R_h) of PLG-*g*-mPEG/Epo906 micelles (Epo906-M) measured by DLS was 47.4 ± 19.1 nm, and the diameter determined by the TEM was around 80.0 ± 28 nm (Figure 4). Nanoparticles with such a size can be retained in the blood circulation system and accumulate in solid tumors after intravenous administration via the leaky vasculature by the EPR effect (<400 nm) [32], that indicating the Epo906-M has a great potential to passively target to solid tumors.
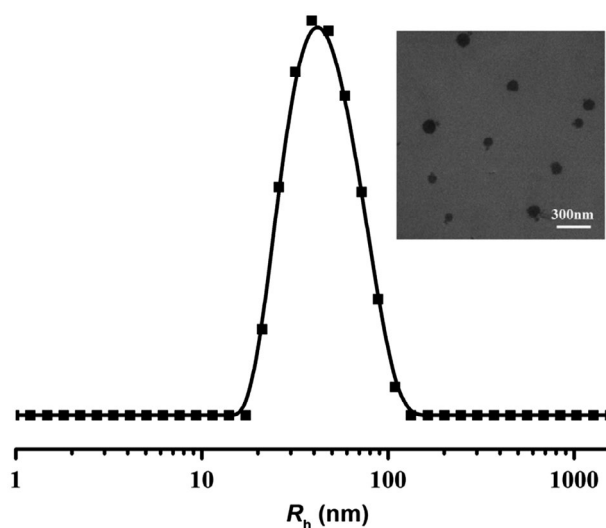
Figure 4. Hydrodynamic radius distribution and typical morphology of Epo906-M in aqueous solution estimated by DLS and TEM, respectively.
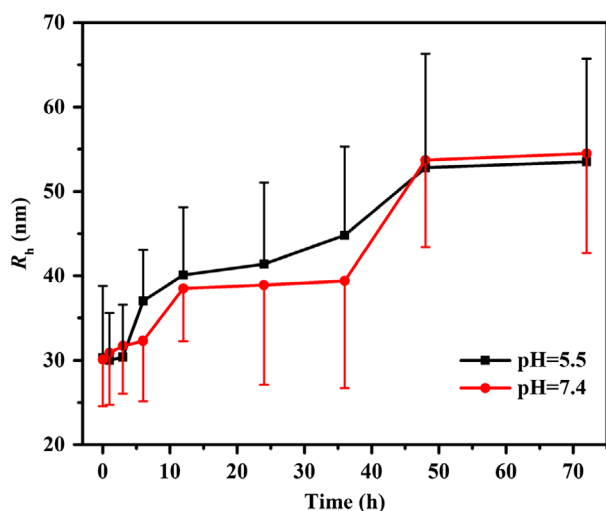

Figure 5. Stability of the Epo906-M in phosphate buffer saline at pH 5.5 and 7.4 at 37 °C.
Note: The data was obtained using DLS ($n = 3$).

The change of the hydrodynamic radius can be used to evaluate the stability of the Epo906-M micelles. As shown in Figure 5, the R_h of the Epo906-M micelles gradually increases at pH 5.5 and 7.4 in 72 h. This indicates that the Epo906-M is not stable in physiological conditions.

3.2. Cell uptake study

Cellular internalization of nanomedicines is crucial for oncotherapy. In this study, cellular uptake was studied by CLSM and FACS. The FITC-labeled PLG-*g*-mPEG/Epo906, prepared
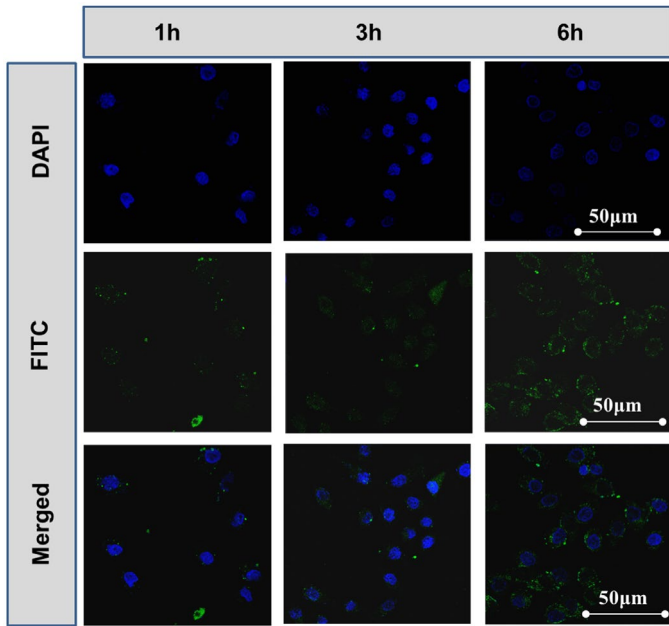
Figure 6. Confocal laser scanning microscopy images with MCF-7 cells after incubation with FITC-labeled PLG-*g*-mPEG/Epo906 for 1, 3 or 6 h.
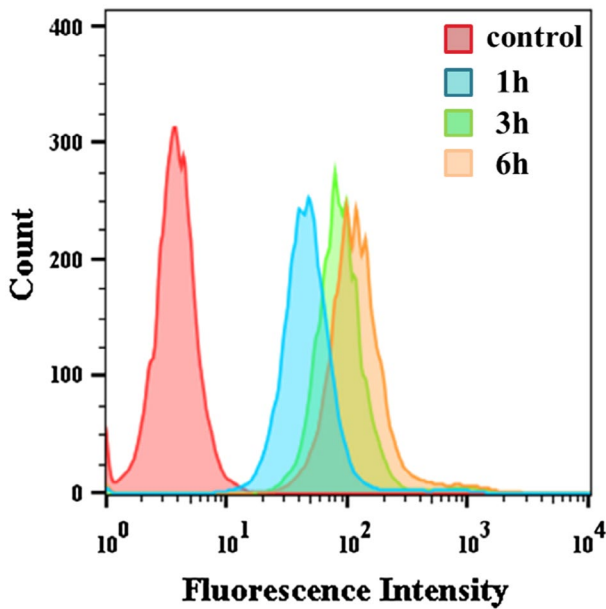

Figure 7. Cell uptake of FITC-labeled PLG-*g*-mPEG/Epo906 after incubation with MCF-7 cells for 1, 3 or 6 h by FACS.
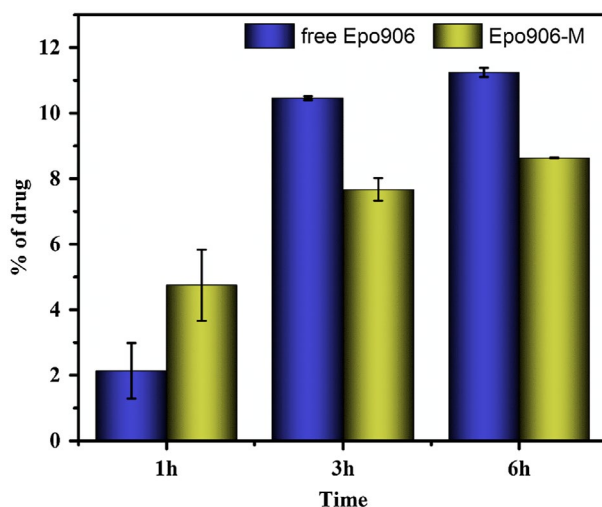
Figure 8. Quantification of cell uptake for PLG-*g*-mPEG/Epo906 and free Epo906 after incubation with MCF-7 cells for 1, 3 or 6 h by HPLC (*n* = 3).

by the reaction of FITC with PLG-g-mPEG/Epo906 (Scheme 1(B)), was cultivated with the MCF-7 cells for 1, 3 or 6 h at 37 °C.

As shown in Figure 6, the cell nuclei of MCF-7 cells were selectively stained with DAPI (blue). Green fluorescence imaging was utilized to visualize FITC. FITC-labeled PLG-*g*-mPEG/Epo906 could be uptaken by MCF-7 cells. A time dependent manner was observed for the cellular accumulation of the FITC-labeled PLG-*g*-mPEG/Epo906 (1 h < 3 h < 6 h).

FACS results were consistent with those obtained by CLSM. As showed in Figure 7, the fluorescent intensity of MCF-7 cells at 6 h was higher than that at 3 h, and both were much stronger than that at 1 h.

A quantification of cell uptake study was shown in Figure 8. For the Epo906-M, the quantification results were consisted with the CLSM and FACS. Compared with the free Epo906, the endocytosis rate of Epo906-M was faster in 1 h, but slower in 3 and 6 h. A time dependent manner was also observed for the cellular uptake of free Epo906. The results of CLSM, FACS and the quantification of cell uptake study indicated that the Epo906-M micelles could be successfully endocytosed by MCF-7 cells.

3.3. In vitro *cytotoxicity assay*

The cytotoxicities of free Epo906 and Epo906-M were estimated with MCF-7, A549 and BEAs-2B cells by MTT assays. As shown in Figure 9, both free Epo906 and Epo906-M showed a dose and time dependent cell proliferation inhibition behavior. As for MCF-7 cells (Figure 9(A) and (B)), both free Epo906 and Epo906-M showed high antiproliferative activity. As the drug concentration increased, a higher antiproliferative activity was observed for both free Epo906 and Epo906-M. The cell viability in 72 h was much lower than that in 48 h for both free Epo906 and Epo906-M. Similar results were obtained in A549 and BEAs-2B cells (Figure 9(C)–(F)).

The IC_{50} values were displayed as Table 2, which showed that the Epo906-M had obviously lower cytotoxicity than free Epo906. This was further confirmed by Trypan blue exclusion
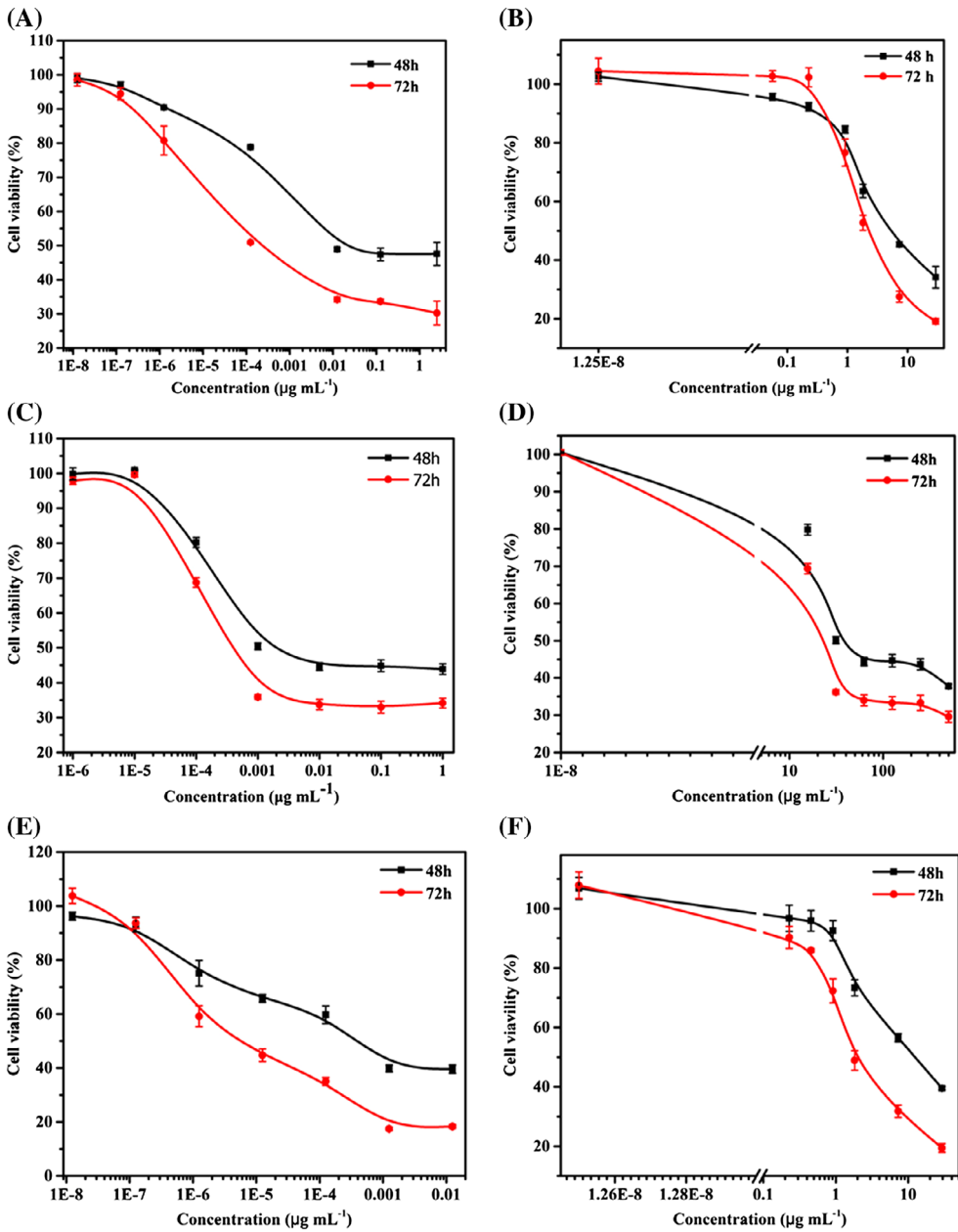
Figure 9. MTT assays of free Epo906 and Epo906-M to MCF-7, A549 and BEAs-2B cells.
Notes: *In vitro* cytotoxicities of free Epo906 to MCF-7 (A), A549 (C) and BEAs-2B cells (E) for 48 or 72 h. *In vitro* cytotoxicities of Epo906-M to MCF-7 (B), A549 (D) and BEAs-2B cells (F) for 48 or 72 h. Data are presented as mean ± standard deviation ($n = 3$).

assay (Table 3). This is reasonable because Epo906 is conjugated to PLG-*g*-mPEG by ester bonds in the Epo906-M. The IC$_{50}$ values of free Epo906 to BEAs-2B cells is extremely low and is much lower than other two cells. This maybe a hint that free Epo906 have severe toxicity to lung.

Table 2. IC$_{50}$ values of different drug formulations against A549 cells, MCF-7 cells and BEAs-2B cells for 48 or 72 h incubation time.

Drugs	Incubation time (h)	IC$_{50}$/(μg mL^{-1}) A549	IC$_{50}$/(μg mL^{-1}) MCF-7	IC$_{50}$/(μg mL^{-1}) BEAs-2B
Free Epo906	48	1.97×10^{-3}	2.02×10^{-2}	4.00×10^{-4}
	72	3.54×10^{-3}	2.53×10^{-4}	5.73×10^{-6}
Epo906-M	48	9.91	5.34	12.50
	72	3.17	2.29	2.05

Table 3. Cell viability of free Epo906 and Epo906-M to MCF-7 cells for 48 h incubation time determined by Trypan blue exclusion assay.

	Free Epo906			Epo906-M		
Concentration (μg mL^{-1})	2.0	2.0×10^{-3}	2.0×10^{-4}	10	3.0	0.55
Cell viability (%)	37.84	52.85	74.47	43.21	57.30	86.36

3.4. In vivo *distribution*

For the *in vivo* distribution study of Epo906-M by MSOT, IR830-labeled PLG-*g*-mPEG/Epo906 was prepared by the reaction of PLG-*g*-mPEG/Epo906 with IR830-B-NH$_2$ (Scheme 1(C)). As shown in Figure 10A, the maximum UV–vis absorbance of the IR830-labeled PLG-*g*-mPEG/Epo906 was at 835 nm, which was similar to the IR830-B-NH$_2$ [36], indicating that the IR830-labeled conjugate could be used for photoacoustic imaging. Quantitative photoacoustic signal intensity of IR830-labeled PLG-*g*-mPEG/Epo906 in liver, spleen, kidney and tumor was shown in Figure 10(B). After injection for 1 h, a strong IR830 photoacoustic signal was observed in the liver and spleen, and reached the highest at 4 h post injection. The photoacoustic signal in kidney was significantly weak during the period of observation. As for tumors, a gradually increased IR830 photoacoustic signal was observed from 1 to 24 h post injection, reaching maximal at 48 h, and at the end of our observation, in 72 h, the photoacoustic signal was much stronger than that during the first 24 h. 2D overview images were one of the cross section of selected scanning area which could avoid the interference of other sections when observing the viscera. The regions circled with dashed white were the corresponding area of interest. 3D overview images were an overlap of all the cross section of the scanning area, which was benefit for the observation of the distribution of Epo906-M in tumors. The dashed yellow represented the section of tumor. The green signals in the picture were used to visualize IR830, and the appearance and strength of the green signals demonstrated that the IR830-labeled PLG-*g*-mPEG/Epo906 could reach and accumulate in the tumor tissue. Consistent results were observed in the 2D overview MSOT images (Figure 10(C)) and 3D overview MSOT images (Figure 10(D)).

3.5. In vivo *cytotoxicity assay*

Based on the above results, the *in vivo* antitumor efficacy and systemic toxicity of free Epo906 and Epo906-M were further investigated on Balb/C nude female mice bearing orthotopic transplantation MCF-7 tumor. As shown in Figure 11(A), the average tumor volume of PBS treatment group reached approximately 900 mm^3 in 18 days. Unconspicuous
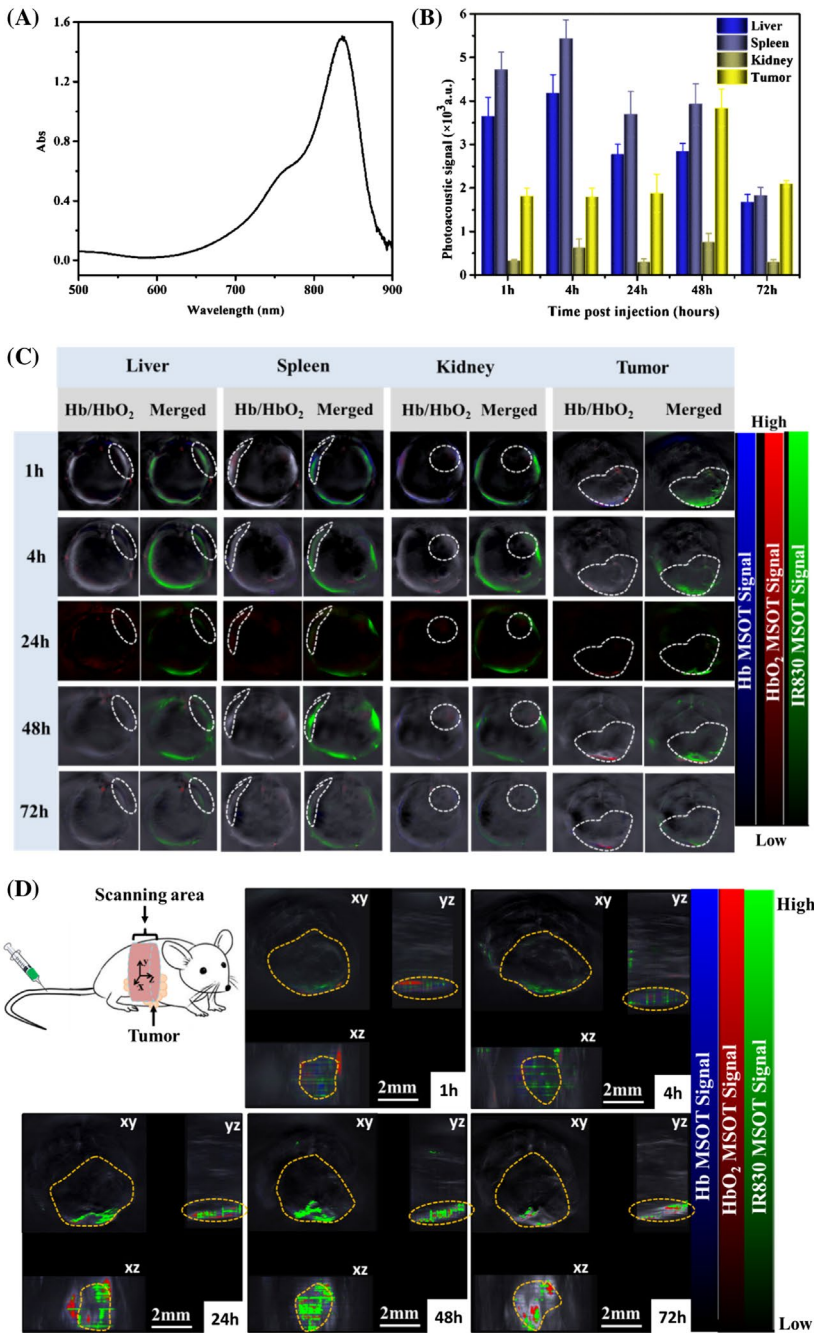
Figure 10. MSOT measurement of MCF-7 tumor-bearing mice at different time intervals after injection of IR830-labeled PLG-*g*-mPEG/Epo906. (A) UV-spectra of IR830-labeled PLG-*g*-mPEG/Epo906 in water, with maximal absorption at 835 nm. (B) Quantitative analysis of IR830 photoacoustic signal intensity in liver, spleen, kidney and tumor ($n = 3$). (C) 2D overview MSOT images of liver, spleen, kidney and tumors. (D) 3D overview MSOT images of tumors. The 3D coordinate system defines the orientations and positions of the orthogonal views.

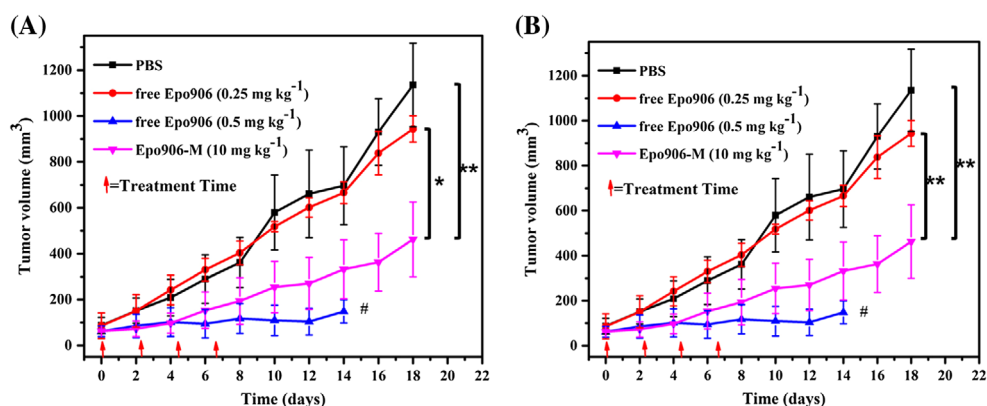Notes: The regions circled with dashed white and yellow lines are relevant area of interest.

(A)

(B)

Figure 11. *In vivo* anti-tumor efficacy of free Epo906 and Epo906-M in term of (A) tumor volume and (B) relative body weight change in MCF-7 orthotopic human breast cancer xenograft-bearing Balb/C nude mice.

Notes: The data are shown as mean ± SD ($n = 6$), *$p < 0.05$, **$p < 0.01$ (one-way ANOVA), # represented the day that the experiment was ended as 50 % of the mice died.

inhibiting efficiency on tumor growth was observed for the treatment of free Epo906 at a dose of 0.25 mg kg^{-1} as compared to the PBS group. For the group of Epo906-M (10 mg kg^{-1} of free Epo906 equivalent), tumor inhibiting efficiency was between the free Epo906 at a dose of 0.25 mg kg^{-1} and 0.5 mg kg^{-1}. The dose of the Epo906-M was 20 times higher than that of free Epo906 at a dose of 0.5 mg kg^{-1}, but the inhibiting efficiency on tumor growth was lower than that of the latter, which might be due to the high stability of the glutamic acid-Epo906 ester bond or the instability of the 16-membered macrolide of Epo906 *in vivo*.

Body weight changes are an indicator of systemic toxicity of anticancer agents. A slight body weight loss was observed for the PBS treated mice, which might be partly due to the bearing of the tumor. Acute body weight loss (about 25%) was observed in the group treated with free Epo906 at a dose of 0.5 mg kg^{-1}, and nearly 17% of body weight loss was observed in the group treated with free Epo906 at a dose of 0.25 mg kg^{-1}, revealing the tremendous toxicity of free Epo906. Less than 10% of body weight loss was observed in the group of Epo906-M (10 mg kg^{-1} of Epo906 equivalent) (Figure 11(B)), revealing the reduced systemic toxicity of the polypeptide-patupilone conjugate. Because the Epo906-M (10 mg kg^{-1} of Epo906 equivalent) showed higher anticancer efficacy and lower systemic toxicity than free Epo906 (0.25 mg kg^{-1}), the Epo906-M has greater potential than free Epo906 for oncotherapy.

3.6. Histopathology analysis

To further evaluate the anti-tumor efficacy and toxicities of free Epo906 and Epo906-M, MCF-7 orthotopic tumor-bearing nude mice were sacrificed at the end of the treatment, the tumor sections were prepared for pathology analysis.

By H&E staining, nuclei were stained bluish violet by hematoxylin, while cytoplasm and extracellular matrix were stained pink by eosin in normal tissues. For necrotic cells, cell morphology was unclear, chromatin became darker or diffused extracellularly, nuclei
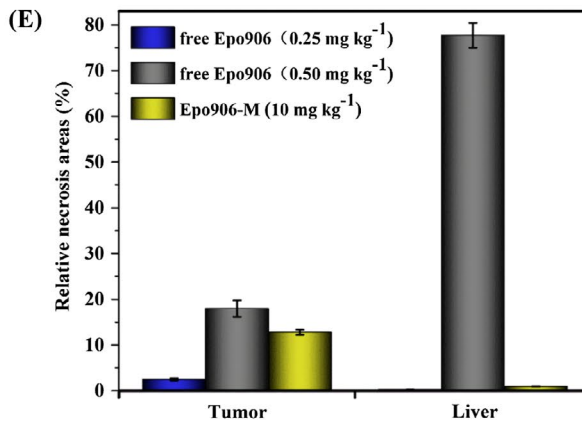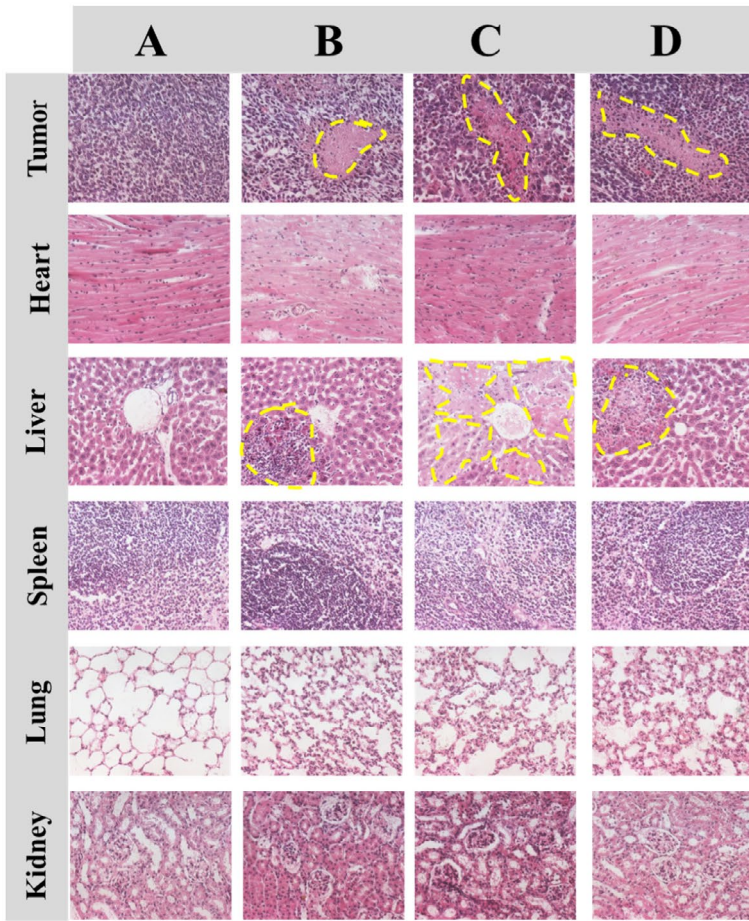
Figure 12. Ex vivo histological of MCF-7 tumor sections and organs. (18 days after the first treatment).
Notes: Nuclei were stained bluish violet, whereas extracellular matrix and cytoplasm were stained pink in H&E staining. The dashed yellow lines marked the necrocytosis area of tissues. (A) PBS; (B) Free Epo906 of 0.25 mg kg^{-1}; (C) Free Epo906 of 0.50 mg kg^{-1}; (D) Epo906-M (equivalent free Epo906 of 10 mg kg^{-1}). (E) Quantification of the necrosis area for tumor and liver ($n = 3$). Relative necrosis area = Necrosis area in each slice / Total area of the slice.

became pyknotic or absent. As is shown in Figure 12, tumor cells of PBS group (A) have clear cell morphology with chromatin, in contrast, tumor cells of the free Epo906 (B and C) and Epo906-M groups exhibited obvious necrosis. Significant liver cell damage was observed in the group treated with 0.50 mg kg^{-1} free Epo906 (C), while the group of 0.25 mg kg^{-1} free Epo906 (B) and 10 mg kg^{-1} Epo906-M (D) displayed reduced liver cell necrotic. The necrotic degree of liver cells had a tendence of C > B > D. As for lung, compared with PBS group (A), the morphological changes of alveolar could be observed for B, C and D, and showed a thicker alveolar wall. These indicated lung damage [23]. From Figure 12(E), almost 80 % of the liver damaged for the 0.5 mg kg^{-1} free Epo906 treatment group, however, negligible liver cells damage was observed in the groups of 0.25 mg kg^{-1} free Epo906 and the 10 mg kg^{-1} Epo906-M. As for the tumor necrosis, the necrosis area of 10 mg kg^{-1} Epo906-M group was more than 5 times higher than that of the free Epo906 of 0.25 mg kg^{-1}, and for free Epo906, the necrosis area of 0.5 mg kg^{-1} is about 7 times higher than 0.25 mg kg^{-1}. For other organs, no significant pathological changes were observed. These results further demonstrated that the Epo906-M had lower systematic toxicity than free Epo906 at some extent.

4. Conclusions

A polypeptide-patupilone conjugate PLG-*g*-mPEG/Epo906 was prepared by Steglich ester-ification reaction with high efficiency. The conjugate can self-assemble to form micelles Epo906-M with R_h of 47.4 ± 19.1 nm in aqueous solution. The Epo906-M can be efficiently uptaken by cancer cells and shows a concentration and time dependent cytotoxicity *in vitro*. The Epo906-M can accumulate in MCF-7 tumors by EPR effect and displays higher anticancer efficacy and lower systemic toxicity than free Epo906 in a proper dose. Therefore, the Epo906-M has greater potential for oncotherapy.

Disclosure statement

No potential conflict of interest was reported by the authors.

ORCID

Jing Yan   http://orcid.org/0000-0001-9154-1408

References

[1] Vicente JJ, Wordeman L. Mitosis, microtubule dynamics and the evolution of kinesins. Exp Cell Res. 2015;334:61–69.

[2] Dumontet C, Jordan MA. Microtubule-binding agents: a dynamic field of cancer therapeutics. Nat Rev Drug Discovery. 2010;9:790–803.

[3] Klar W, Ka U. Differences and similarities of epothilones. Curr Cancer Ther Rev. 2011;10–36.

[4] Khade P, Giannakakou P. 4E-BP1 hyper-phosphorylation senses microtubule damage and plays a critical role in taxane antitumor activity. Cancer Res. 2016;76:2896.

[5] Gong G-L, Huang Y-Y, Liu L-L, et al. Enhanced Production of Epothilone by Immobilized Sorangium cellulosum in Porous Ceramics. J. Microbiol Biotechnol. 2015;25:1653–1659.

[6] An F, Zhao W-J, Tang L, et al. Concentration-dependent differential effects of an epothilone analog on cell cycle and p53 signaling. Oncol Rep. 2015;34:1361–1368.

[7] Bollag DM, M PA, Zhu J, et al. Epothilones, a new class of microtubule-stabilizing agents with a taxol-like mechanism of action. Cancer Res. 1995;55:2325–2333.

[8] Colombo N, Kutarska E, Dimopoulos M, et al. Randomized, open-Label, phase III study comparing patupilone (EPO906) with pegylated liposomal doxorubicin in platinum-refractory or -resistant patients with recurrent epithelial ovarian, primary fallopian tube, or primary peritoneal cancer. J Clin Oncol. 2012;30:3841–3847.

[9] Castonguay V, Wilson MK, Diaz-Padilla I, et al. Estimation of expectedness: predictive accuracy of standard therapy outcomes in randomized phase 3 studies in epithelial ovarian cancer. Cancer. 2015;121:413–422.

[10] Wartmann M. AK-H. The biology and medicinal chemistry of epothilones. Curr Med Chem. 2002;2(123–148):123–148.

[11] Ferretti S, Allegrini PR, O'Reilly T, et al. Patupilone induced vascular disruption in orthotopic rodent tumor models detected by magnetic resonance imaging and interstitial fluid pressure. Clin Cancer Res. 2005;11:7773–7784.

[12] O'Reilly T, Wartmann M, Brueggen J, et al. Pharmacokinetic profile of the microtubule stabilizer patupilone in tumor-bearing rodents and comparison of anti-cancer activity with other MTS in vitro and in vivo. Cancer Chemother Pharmacol. 2008;62:1045–1054.

[13] Rothermel J, Wartmann M, Chen T, et al. EPO906 (epothilone B): a promising novel microtubule stabilizer. Semin Oncol. 2003;30:51–55.

[14] Bukowska B, Rogalska A, Marczak A. New potential chemotherapy for ovarian cancer – combined therapy with WP 631 and epothilone B. Life Sci. 2016;151:86–92.

[15] Broggini-Tenzer A, Sharma A, Nytko KJ, et al. Combined treatment strategies for microtubule stabilizing agent-resistant tumors. JNCI J Natl Cancer Inst. 2015;107:dju504.

[16] Dorkoosh F, Dehghankelishadi P, Samimi S. Paclitaxel delivery systems; from a stubborn undruggable to an efficient chemotherapeutic in clinic. SM J Clin Pharm Acta. 2015;1:1002.

[17] Wang L, Cai M, Liu Y, et al. Polymer hydrophobicity regulates paclitaxel distribution in microspheres, release profile and cytotoxicity in vitro. Powder Technol. 2015;275:77–84.

[18] Hamaguchi TM, Suzuki Y, Shimizu M, et al. NK105, a paclitaxel-incorporating micellar nanoparticle formulation, can extend in vivo antitumour activity and reduce the neurotoxicity of paclitaxel. Br J Cancer. 2005;92:1240–1246.

[19] Bughani U, Li S, Joshi HC. Recent patents reveal microtubules as persistent promising target for novel drug development for cancers. Recent Pat Anti-Infect Drug Discovery. 2009;4(3):164–182.

[20] Hussain A, DiPaola RS, Baron AD, et al. Phase II trial of weekly patupilone in patients with castration-resistant prostate cancer. Ann Oncol. 2009;20:492–497.

[21] Melichar B, Casado E, Bridgewater J, et al. Clinical activity of patupilone in patients with pretreated advanced/metastatic colon cancer: results of a phase I dose escalation trial. Br J Cancer. 2011;105:1646–1653.

[22] Peereboom DM, Murphy C, Ahluwalia MS, et al. Phase II trial of patupilone in patients with brain metastases from breast cancer. Neuro-Oncology. 2014;16:579–583.

[23] Fogh S, Machtay M, Werner-Wasik M, Jr., et al. Phase I trial using patupilone (epothilone b) and concurrent radiotherapy for central nervous system malignancies. Int J Radiat Oncol Biol Phys. 2010;77:1009–1016.

[24] Feng T, Xiao Z, Geng L, et al. Stereocomplex micelle efficiently transports Doxorubicin for enhanced lymphoma suppression in vivo. J Biomater Sci Polym Ed. 2016;27:1–20.

[25] Li Y-f, Yu H-y, Sun H, et al. Cisplatin-loaded poly(L-glutamic acid)-g-methoxy poly(ethylene glycol) nanoparticles as a potential chemotherapeutic agent against osteosarcoma. Chin J Polym Sci. 2015;33:763–771.

[26] Siddalingappa B, Benson HA, Brown DH, et al. Stabilization of resveratrol in blood circulation by conjugation to mpeg and mpeg-pla polymers: investigation of conjugate linker and polymer composition on stability, metabolism, antioxidant activity and pharmacokinetic profile. PLoS One. 2015;10:e0118824.

[27] Näkki S, Rytkönen J, Nissinen T, et al. Improved stability and biocompatibility of nanostructured silicon drug carrier for intravenous administration. Acta Biomater. 2015;13:207–215.

[28] Liang H, Friedman JM, Nacharaju P. Fabrication of biodegradable PEG–PLA nanospheres for solubility, stabilization, and delivery of curcumin. Artif Cell Nanomed Biotechnol. 2016;1–8.

[29] Maeda H, Tsukigawa K, Fang J. A retrospective 30 years after discovery of the enhanced permeability and retention effect of solid tumors: next-generation chemotherapeutics and photodynamic therapy – problems, solutions, and prospects. Microcirculation. 2016;23:173–182.

[30] Yu Q, Wei Z, Shi J, et al. Polymer-doxorubicin conjugate micelles based on poly (ethylene glycol) and poly (N-(2-hydroxypropyl) methacrylamide): effect of negative charge and molecular weight on biodistribution and blood clearance. Biomacromolecules. 2015;16:2645–2655.

[31] Chen H, He S. PLA–PEG coated multifunctional imaging probe for targeted drug delivery. Mol Pharm. 2015;12:1885–1892.

[32] Maeda H, Wu J, Sawa T, et al. Tumor vascular permeability and the EPR effect in macromolecular therapeutics: a review. J Contr Release. 2000;65:271–284.

[33] Peer D, Karp J, Hong S, et al. Nanocarriers as an emerging platform for cancer therapy. Nat Nanotechnol. 2007;2:751–760.

[34] Ahmad Z, Lv S, Tang Z, et al. Methoxy poly (ethylene glycol)-block-poly (glutamic acid)-graft-6-(2-nitroimidazole) hexyl amine nanoparticles for potential hypoxia-responsive delivery of doxorubicin. J Biomater Sci Polym Ed. 2016;27:40–54.

[35] Zhang H, Wang K, Cheng X, et al. Synthesis and In vitro cytotoxicity of poly (ethylene glycol) – epothilone B conjugates. J Appl Polym Sci. 2014;131.

[36] Niu Y, Song W, Zhang D, et al. Functional computer-to-plate near-infrared absorbers as highly efficient photoacoustic dyes. Acta Biomater. 2016;43:262–268.

[37] Song W, Tang Z, Li M, et al. Tunable pH-sensitive poly(beta-amino ester)s synthesized from primary amines and diacrylates for intracellular drug delivery. Macromol. Biosci. 2012;12:1375–1383.

[38] Song W, Tang Z, Shen N, et al. Combining disulfiram and poly(l-glutamic acid)-cisplatin conjugates for combating cisplatin resistance. J Contr Release. 2016;231:94–102.

[39] Yu H, Tang Z, Zhang D, et al. Pharmacokinetics, biodistribution and in vivo efficacy of cisplatin loaded poly(l-glutamic acid)-g-methoxy poly(ethylene glycol) complex nanoparticles for tumor therapy. J Contr Release. 2015;205:89–97.

[40] Shi C, Yu H, Sun D, et al. Cisplatin-loaded polymeric nanoparticles: Characterization and potential exploitation for the treatment of non-small cell lung carcinoma. Acta Biomater. 2015;18:68–76.

[41] Song W, Tang Z, Zhang D, et al. Anti-tumor efficacy of c(RGDfK)-decorated polypeptide-based micelles co-loaded with docetaxel and cisplatin. Biomaterials. 2014;35:3005–3014.

[42] Yu H, Tang Z, Li M, et al. Cisplatin loaded poly(L-glutamic acid)-g-methoxy poly(ethylene glycol) complex nanoparticles for potential cancer therapy: preparation, in vitro and in vivo evaluation. J Biomed Nanotechnol. 2016;12:69–78.

[43] Song W, Tang Z, Zhang D, et al. Solid tumor therapy using a cannon and pawn combination strategy. Theranostics. 2016;6:1023–1030.

[44] Song W, Tang Z, Zhang D, et al. A cooperative polymeric platform for tumor-targeted drug delivery. Chem Sci. 2016;7:728–736.

[45] Yifei L, Hai-yang Y, Sun H, et al. Cisplatin-loaded poly(L-glutamic acid)-g-methoxy poly(ethylene glycol) nanoparticles as a potential chemotherapeutic agent against osteosarcoma. Chin J Polym Sci. 2015;33:763–771.